MTLA 30 (2023) 101855

Contents lists available at ScienceDirect

Materialia

journal homepage: www.elsevier.com/locate/mtla

Modelling of the hydrogen embrittlement in austenitic stainless steels

Pasquale Cavaliere *, Angelo Perrone, Debora Marsano, Antonio Marzanese, Behzad Sadeghi

Department of Innovation Engineering, University of Salento, Via per Arnesano 73100 Lecce-Italy

ARTICLE INFO

Keywords:
Hydrogen embrittlement
Traps
Microstructure
Finite element modelling
Diffusion

ABSTRACT

The paper shows the 3D model of hydrogen diffusion in austenitic stainless steel. To model the behaviour of the material a real microstructure of grain boundaries, of dislocation density, of number of vacancy and the states of precipitates is taking in account and implemented in the software (ANSYS). The effect of each single hydrogen trap was physically determined. To improve the affordability of the results a high number of elements and nodes were carried out in the simulation. The purpose of the model is to identify the hydrogen diffusion in different conditions evaluating the weight of each trap in the process. The model allowed to define the hydrogen saturation of the microstructure in different temperature conditions. The results showed that the trapping effect of vacances is negligible at room temperature and their effect increases as the diffusion temperature increases. The main trapping effect is experienced by the grain boundary then by dislocations and then by the lattice. The trapping effect of precipitates has a remarkable dependence on their dimensions.

1. Introduction

Hydrogen adsorption in metals lead to a ductility decrease, this phenomenon is called hydrogen embrittlement (HE), or hydrogen-assisted cracking or hydrogen-induced cracking (HIC). The little size of hydrogen atoms makes them capable to penetrate the solid metals. Adsorbed hydrogen reduces the force necessary to begin and spread crack in the metal, this comes into embrittlement [1,2]. Steels, iron, nickel, titanium, cobalt and their alloys are susceptible to hydrogen embrittlement [3,4].

Embrittlement due to hydrogen is dependent from temperature [5, 6]. Most metals are mildly resistant to hydrogen embrittlement when temperature is above 150 °C [7]. To have hydrogen embrittlement the contemporary existence of hydrogen atoms (``diffusible'') and a mechanical stress that cause fracture formation is needed [8–10]. High strength materials are more brittle due to hydrogen embrittlement [11–12]; this is due to the fact that materials are strengthened through strain gardening (inducing high dislocations density), precipitation hardening (inducing high density of precipitates), grain refining (inducing high density of grain boundaries); these are all microstructural features contributing to increase the trapping of hydrogen atoms.

Metals' surfaces can be expose to hydrogen in two ways: by gaseous hydrogen and by chemical produced hydrogen. Gaseous hydrogen is molecular, and it doesn't cause embrittlement because it dissolves into metal at ambient temperature; the atom hydrogen from chemical assault that causes embrittlement [13,14]. Hydrogen can be produced electrochemically by acid, corrosion and electroplating processes [15,16]. Pipelines and pressure vessels contain gaseous hydrogen.

The hydrogen embrittlement phenomena depend on how the atoms diffuse into the steel microstructure. Hydrogen diffuse trough metals (by normal interstitial site or by dislocation transport) easily because it is the smallest chemical element, and when diffuse the metals become brittle [17,18].

Hydrogen trapping defect are important to diffusion process. Dislocation, grain boundaries, precipitates and other defects are called traps. Even the small traps have impact in diffusivity due to rapid diffusion of hydrogen [19,20].

McNabb and Foster [21] presented the first model of dissolved mobility of hydrogen in an iron lattice with trapping sites, that brings a diffusion equation in terms of sources and sinks. Oriani [9] modified the model introducing the equilibrium between the mobile and the trapped hydrogen for a constrained region.

1.1. Hydrogen diffusion and trapping models

Diffusion is the process that brings matter into another material due to molecular motions. During diffusion hydrogen can occupied interstitial lattice sites or atomic and microstructural defects: vacancies, grain boundaries, voids, dislocations, cracks, etc. [22]. Atomic hydrogen can recombine to gaseous hydrogen in voids or crack into metals [23,

* Corresponding author.
E-mail address: pasquale.cavaliere@unisalento.it (P. Cavaliere).

https://doi.org/10.1016/j.mtla.2023.101855
Received 9 December 2022; Accepted 20 July 2023
Available online 21 July 2023

24]. Dislocations and grain boundaries can contain a definite number of atomic hydrogen, for this reason this traps are called ``saturable traps'' [25,26]. In a theorical defect-free microstructure hydrogen can diffuse into it jumping from an interstitial site to another due to its small size. To do that jump a sufficient activation energy E_a is needed to overcome the energetic barrier. It's possible to estimate the hydrogen volume concentration in lattice sites. It is assumed that hydrogen atoms diffuse into lattice according to Fick's law that is in steady state (time-dependency is neglected) (Eq. (1))

$$\overline{J} = D_L * \nabla C_L \tag{1}$$

Where $\overline{J}$ is the hydrogen flux vector, D_L is the hydrogen lattice diffusion coefficient and C_L is the hydrogen concentration in lattice sites. The hydrogen diffusion coefficient is function of temperature, position and time and it is calculated (for simplicity) by Arrhenius-like relationship (Eq. (2)):

$$D_L = D_{L_0} * \exp\left(-\frac{E_a}{RT}\right) \tag{2}$$

where D_{L_0} is the pre-exponential factor, R is the universal gas constant, T is the absolute temperature, and E_a is the activation energy needed to move between two adjacent lattice sites.

Hydrostatic stress gradient, σ_H, due to stress of the material, helps the hydrogen diffusion trough regions with high σ_H. In this case the Eq. (2) became the Eq. (3) [27]:

$$\overline{J} = -D_L * \nabla C_L + \frac{D_L V_H C_L}{RT} \nabla \sigma_H \tag{3}$$

where V_H is the partial molar volume of hydrogen.

In the diffusion process the number of hydrogen atoms is conserved. In a transient diffusion process hydrogen concentration can change over time at any location, so the Eq. (1) must be change considering the variation on hydrogen flux: the gradient of hydrogen exiting at the exit surface is descripted by Eq. (4):

$$\frac{\partial \overline{J}}{\partial x} dx = J_{OUT} - J_{IN} \tag{4}$$

By assuming that the hydrogen diffusion coefficient is constant, the variation of the concentration over the time is expressed by Eq. (5).

$$\frac{\partial C_L}{\partial t} = -\nabla * \overline{J} = D_L \nabla^2 C_L \tag{5}$$

In presence of mechanical stresses Eq. (5) becomes Eq. (6):

$$\frac{\partial C_L}{\partial t} = D_L \nabla^2 C_L + D_L \nabla * \left(\frac{V_H C_L}{RT} \nabla \sigma_H\right) \tag{6}$$

A site in which the hydrogen chemical potential is lower than the one in the interstitial site is considering a trap from a thermodynamic point of view. The microstructural imperfection like vacancies, dislocations and etc. are considered as hydrogen traps because they raise the activation energy that is needed to break through the energetic barrier. The most predominant defect are grain boundaries that favourite the hydrogen transportation because its create a diffusion path, especially in those with high misorientations. Diffusion, in fact, is accelerated in the boundary grains [28]. The effect of boundary grain is important due to its high presence in metals lattice [29]. Hydrogen easily occupies the vacancies in the metals, and the amount of hydrogen atoms that can stay in this defect is proportional to vacancy size. The trapping in the vacancies lead to a hydrogen diffusion coefficient decreasing [30,31]. Plastic deformation and grain growth processes produced linear defects, called dislocation. These defects cause distortion of the crystal lattice and hydrostatic stresses development to the core of dislocation [32]. Dislocations generate a lot of trap sites, with different energies of trapping and act as a reversible trap at the edge and as irreversible trap at the core [33]. The uptake and desorption behaviours of hydrogen is dependent on the quantity and size of precipitates, whose size is proportional to the amount of hydrogen that can be trapped in it.

As says before most diffusion models are based on hydrogen diffusion refer to the mathematical model of McNabb & Foster and Oriani reformulated the model using local equilibrium hypotheses. But it's important to modify the previous Fick's laws to considering the traps.

C_T is the hydrogen volume concentration in trap sites. By considering C_T greater than zero, Eq. (5) becomes Eq. (7):

$$\frac{\partial (C_L + C_T)}{\partial t} = -\nabla \overline{J} \tag{7}$$

If D_L is assumed constant in the material, Eq. (7) can be modified as Eq. (8):

$$\frac{\partial C_L}{\partial t} + \frac{\partial C_T}{\partial t} = D_L \nabla^2 C_L \tag{8}$$

In presence of mechanical stresses Eq. (9):

$$\frac{\partial C_L}{\partial t} + \frac{\partial C_T}{\partial t} = D_L \nabla^2 C_L + D_L \nabla * \left(\frac{V_H C_L}{RT} \nabla \sigma_H\right) \tag{9}$$

The equation formulated by McNabb and Foster is the following Eq. (10):

$$\frac{\partial \theta_T}{\partial t} = k C_L (1 - \theta_T) - p \theta_T \tag{10}$$

Where, θ_T is the fractional occupancy of traps, k and p are two parameters that describe the trapping effect. In particular: k is related to the hydrogen atoms captured per second and p is related to the probability that a trap containing a hydrogen atom will release it in one second.

The parameters k and p are function of temperature according to Arrhenius relationships [34]: (Eq. (11)) (Eq. (12)).

$$k = k_0 \exp\left(-\frac{E_t}{RT}\right) \tag{11}$$

$$p = p_0 \exp\left(-\frac{E_d}{RT}\right) \tag{12}$$

where Et is the diffusion sites energy and Ed is the trapping energy of the site. Oriani reformulated this model by assuming that the hydrogen concentration in trap sites C_T depends only on the hydrogen concentration in lattice sites. The equilibrium between the two population is described by the constant K: (Eq. (13)).

$$K = \frac{1 - \theta_L}{\theta_L} \left(\frac{\theta_T}{1 - \theta_T}\right) \tag{13}$$

Θ_L is the occupancy of lattice sites. N_L and N_T are the available sites.

To determine material hydrogen diffusion coefficient electrochemical techniques are used. During that tests metallic specimens are used to obtain the trend of that membrane permeation as a function of time. The flux permeation i_∞ can be defined as the hydrogen diffusion across the membrane supposing that the hydrogen entering the steel surface is an adsorption-absorption reaction within local equilibrium reaction.

It is assumed as boundary condition that the amount of hydrogen in the specimens rises over time, this lead to a permeation current density rising measured at the exit surface, in which zero hydrogen concentration means that hydrogen totally completed oxidation.

At steady state to the transient, the permeation reaches its maximum and the concentration of hydrogen permeation is linear and flat and does not change with time. The hydrogen permeation or the current density is given at the final state by Eq. (14):

$$\Delta i_\infty = \frac{F D_L C_0}{d} \tag{14}$$

where D_L is the effective hydrogen diffusion coefficient, C_0 is the

hydrogen subsurface concentration, and d is the membrane thickness, F is the Faraday's constant.

The hydrogen flux or permeation rate is directly related to the hydrogen subsurface concentration at the cathodic side due to the difference in hydrogen concentration between the entry surface and the exit surface of the specimen. It is experimentally determined by using the Eq. (15).

$$J = \frac{\Delta i_{\infty}}{F} = \frac{D_L C_0}{d} \tag{15}$$

where J represents the hydrogen flow across the steel specimen. After permeation experiments have produced findings for the hydrogen transient curve dependent on time quantitative analysis can be used to assess hydrogen diffusion coefficients:

1 Inflection point method
2 Breakthrough time method
3 Time lag method

Important to hydrogen atoms transport is the crystal structure of the material [35,36]. The bcc-crystal (body centred cubic) structure and the fcc-crystal (face centred cubic) structure offer interstitial sites with different behaviours for foreign atoms (like hydrogen), so it is important to understand the properties of the iron matrix lattice crystal structures.

The interstitial sites can be categorised into two groups:

1 tetrahedral interstices
2 octahedral interstices

There are two different interstitial locations in the fcc-crystal system that can contain a smaller atom of another element. The hole at the cube's core and the cores on the cube's edge are examples of the larger form of interstice. It is surrounded by six atoms in the fcc lattice at the corners of a regular octahedron.

The smallest crystal system is the fcc-crystal system is the tetrahedral interstice surrounded by four atoms.

Compared to the fcc-crystal system, the bcc-crystal system is less densely packed. There are two different types of interstices in the BCC system.

Tetrahedral interstice is the first type. The second type is smaller than the first and it's the octahedral interstice.

Hydrogen solubility diffusion is affected by the characteristic of interstices. Hydrogen solubility in fcc-crystal is higher than in a bcc-crystal. In fcc-lattice materials, Octahedral interstitial places are larger than tetrahedral ones, while in bcc-lattice materials, Tetrahedral interstice places are larger one instead of Octahedral ones.

As mentioned from the previous paragraph the diffusivity of hydrogen depends on the type of lattice. In addition, the volume of hydrogen generates distortions in unstrained lattices. Hydrogen atoms fill the interstitial space in the lattice and modify the electronic structure of metal atoms. This led to a decrease in the interatomic cohesion and bring embrittlement effect [37].

Embrittlement mechanism is an interaction between diffusion of hydrogen, stress field and microstructure. To characterize the phenomena four theories were formulated:

- Hydride Induced Embrittlement
- Hydrogen Induced Decohesion
- Hydrogen Dislocation Interaction
- Hydrogen Vacancy Interaction

The oversaturation of hydrogen promotes the formation of a second phase called metal hydride [38,39]. The presence of this phase in the crack tip can led to cracking. Depending on the hydride potential there are four groups of hydrides that could be formed:

1 1 ionic hydrides (that have salt-like characteristic);
2 transition hydrides;
3 intermediate hydrides;
4 covalent hydrides.

This mechanism can be seen in iron alloys such as austenitic steels. Iron and ferritic alloys are not affected by this mechanism due to the low hydrogen solubility that does not able to form hydride.

Atomic hydrogen accumulated in the lattice decreases the interatomic cohesion forces. The accumulation is due to the hydrostatic stress that dilatates the lattice or by trapping mechanism, the prevalent contribute [40]. Larger hydrostatic-shear stresses will lead to a larger accumulation of hydrogen in the crack tip [41,42]. Cracking occurs when the local tensile stresses exceed the cohesion strength.

The assumption for this theory is that the hydrogen changes the dislocation mobility and influences the fracture behaviour of the materials changing the plasticity effect region. The hydrogen's contribute to the dislocation mobility represents both a hardening effect and softening effect depending on material [43,44].

Hardening: hydrogen will interact with the stress field around a dislocation to form a hydrogen cloud. These clouds are called Cottrell-atmosphere and they strongly hinder the movement of a dislocation. The movement of hydrogen cause degradation of the mechanical properties by generating microcracks and changing the work hardening rate.

Softening: hydrogen reduces the fracture strength of the materials in the zone where hydrogen concentration is saturated. When the critical strain is reached the failure will occur.

Hydrogen Enhanced Localised Plasticity (HELP) mechanism is the theory that assumes that hydrogen in solid solution increase the dislocation mobility, which involve to a localized plasticity deformation and to a decrease of the critical stress required for the crack initiation. This theory is the most studied in research.

This theory is based on the generation of new vacancies from hydrogen. These vacancies are called Superabundant Vacancy (SAV) [45].

The SAV formation is due to the interaction between absorbed hydrogen and the already present vacancies in the microstructures. The grow of the vacancies number may generate microcracks or microvoids [46].

In this paper, all these are analysed, and a FEM model is implemented in Ansys capable of simulating the diffusion of hydrogen for a microstructure of austenitic stainless steel.

Using the theories of McNabb & Foster and Oriani, a model is implemented to simulates the interaction between hydrogen atoms and the lattice, understanding the effects of traps.

1.2. Model implementation

To implement the hydrogen transport equation, it's possible to use the similarities whit the heat equation. This similarity allows to simulate the phenomenon of hydrogen diffusion in any FEM software in which this equation is implemented. In this work Ansys Workbench and Mechanical APDL are used.

The heat equation is represented by the following expression (Eq. (16)):

$$\rho c_p \frac{\partial T}{\partial t} + \nabla \cdot \overline{J_q} + r_q = 0 \tag{16}$$

In the heat equation the degree of freedom is the temperature T, the temperature is substituted by the hydrogen concentration in lattice C_L. Density ρ and specific heat c_p in the heat equation are set equal to one in the hydrogen diffusion expression. Whit this manipulation it's possible to set the material conductivity k equal to the hydrogen diffusion coefficient D_L. r_q is the heat source that in the diffusion problem becomes hydrogen source r_m and set equals to zero. J_q is the heat flux that in the diffusion equation becomes the hydrogen flux J.

The heat equation (Eq. (17)): becomes:

$$1 * \frac{\partial C_L}{\partial t} + \nabla \cdot \bar{J} + r_m = 0 \tag{17}$$

In the models the heat equation is used two times to simulate the hydrogen diffusion in two different conditions.

The model was implemented by increasing the degree of complexity. The first model is a 2D pure diffusion problem in a microstructure formed by a single grain and his boundary grain (hexagon). After this step, the traps such as dislocation, precipitates, and vacancies are implemented.

The second model is a 3D pure diffusion problem in a microstructure formed by a single grain and his boundary grain (icosahedron). After this step were implemented the traps such as dislocation, precipitates, and vacancies.

The model is based on an austenitic stainless-steel microstructure whose primary crystalline structure is austenite. Figure 1a shows a micrograph of the austenitic microstructure.

For the selected metal the average area of a single grain is 100 [um^2]. Initially a single grain was analysed and then a more complex one to make the model more efficient. The single grain has a hexagon shape whit an area of 100 [um^2].

The traps that are simulated are of four types: boundary grains, dislocation, precipitates, and vacancies.

Boundary grains have a high impact for the diffusion of hydrogen on metals. These traps are preferential path for the diffusion of hydrogen. In general, the diffusion coefficient of boundary grain in greater than three orders of magnitude than lattice. Boundary grain material is implemented to simulate the effect of the boundary grain. This material has the same mechanical properties of the lattice, but it has different diffusion coefficient. The boundary grains diffusion coefficient is function of the temperature.

The expression (Eq. (18)) of the diffusion coefficient for the grain boundary is:

$$D_{L_{GB}} = D_{L_{0_{GB}}} * \exp\left(-\frac{E_L}{RT}\right) \tag{18}$$

The dimension and the number of the boundary grains are constant for all the temperature.

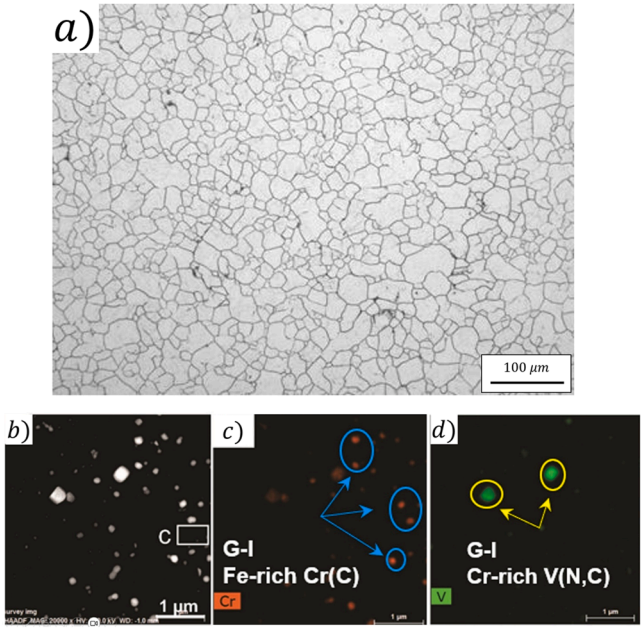

Fig. 1. Micrograph of the austenitic microstructure (a), microanalyses of the precipitates (b-d).

Dislocations are simulated as saturable traps. The number and the diffusive properties of the dislocations are function of the temperature.

Austenitic stainless steel subjected to the extrusion process has a dislocation density equal to 10^{16} $\left[\frac{dislocation}{m^2}\right]$. The number of dislocations is function of temperature is constant for temperature lower than 600 °C. For temperature greater than 600 °C dislocation's number has a linear decreasing trend up to 10^{12} $\left[\frac{dislocation}{m^2}\right]$ for temperature equal to 1000 °C.

To simulate the effect of the dislocations in the diffusion path a specific material was implemented. This material presents the same mechanical properties of the lattice, but the diffusion coefficient, that depends on the temperature, is different. The quantity of hydrogen that saturates the dislocation is set equal to the quantity that saturates the lattice.

Precipitates are modelled as irreversible traps. Four types of precipitates are considered which correspond to different size and composition of the precipitates: The first type (>200 *nm*) that comprises Vanadium carbides and Vanadium nitrides, Type 2A and 2B (=100 *nm*) that comprises Chromium carbides and Iron carbides and type 3 (=20 *nm*) that comprises Chromium nitrides.

Hydrogen diffusion path is highly influenced by the number of precipitates and their size as analysis of thermal desorption spectroscopy (TDS) demonstrated.

Figure 1b-d shows EDX-spectral maps of carbide and nitro-carbide precipitates extracted from. From Fig. 2 it's possible to notated that there are four types of precipitates. The size of the area where the analyses were performed is 18.5 [um^2].

Table 1 summarized the results of the spectral analysis performed on the steel and the amount of total area occupied by precipitates by assuming that the precipitates have a spherical shape.

Each type of precipitate is analysed to discover how many atoms of hydrogen can fill it.

In the first type of precipitates there are: Vanadium carbides (*VC*), it's an extremely hard refractory ceramic material. It has a cubic crystal structure whit a Pearson symbol of cF8. The space group is Fm3m. Vanadium nitride (*VN*), it's formed during the nitriding od steel. It has a cubic crystal structure whit a Pearson symbol of cF8.

These precipitates are formed by Vanadium that is an hard malleable transition metal. Vanadium atoms has an atomic radius of 130 [*pm*]. Nitrogen has an atomic radius of 65 [*pm*]. Carbon has an atomic radius of 70 [*pm*].

The second type of precipitates are formed by Chromium carbides (Cr_3C_2). $Cr_3C_2$is a refractory ceramic material. Its crystal structure is orthorhombic.

These precipitates have an average diameter of 100 [*nm*] The second type of precipitates includes Cementite Fe_3C also. Cementite is a metal carbide which has an orthorhombic structure. It is an hard and brittle material.

The last type of precipitates are the smallest precipitates. In this case there are the Chromium nitride whit particle size of 20 [*nm*], *CN* has a face-cantered cubic structure.

Precipitates are mostly located around the boundary grans. For this reason, the 70% of the precipitates will be implemented in the boundary grain geometry. The remaining fraction will be implemented in the lattice.

Vacancies are characterized by a missing atom in the reticular site. Vacancies can be the result of atomic vibration and its number increase when the temperature increases following the expression (Eq. (19)):

$$N_v = N_0 \exp\left(-\frac{Q_v}{RT}\right) \tag{19}$$

Where N_0 is the total reticular site, N_v is the number of vacancies at equilibrium, R is gas constant, Q_v is the activation energy (vibration energy required) and T is the absolute temperature. In general, for metals, there is a vacancy for 10,000 atoms when the temperature is equal to the fusion temperature.

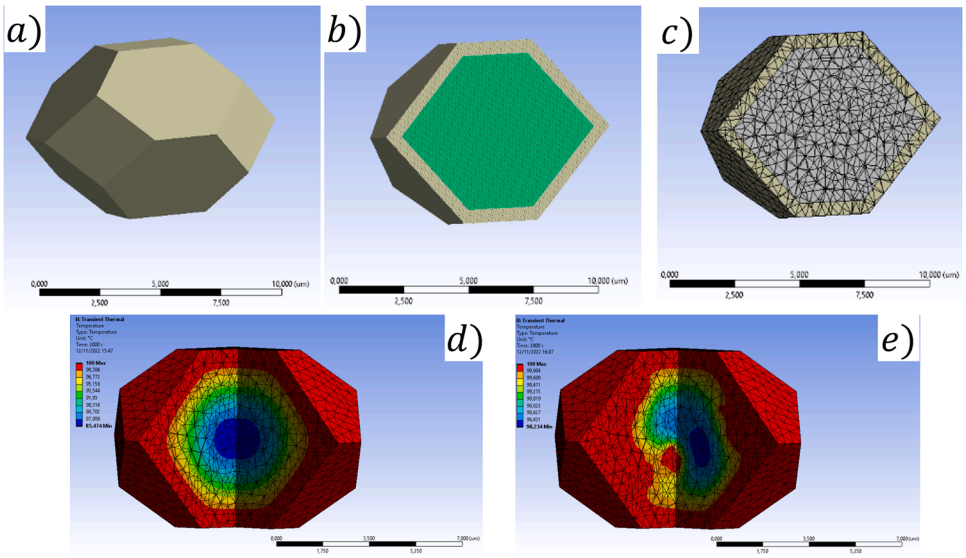

Fig. 2. Geometry and mesh of the 3D model (a–c), thermal analysis nodal results for the 3D model (d), thermal analysis nodal results for the 3D model considering the dislocations effect (e).

Table 1
Summary of the results of the spectral analysis.

Type of precipitate	Average diameter [nm]	Number of precipitates in the reference area	Total area of precipitate in the reference area [um^2]	Normalized percentage of precipitate area
1	323,5	2	164,304,0325	0,89%
2A	147,1	25	424,653,7963	2,30%
2B	97,1	29	214,637,7537	1,16%
3	38,3	49	56,423,92,385	0,31%

The number of mesh element that must simulate the vacancies effect is three orders of magnitude lower than that of the other traps, for this reason the implementation of the vacancies is not executed.

After defining the boundary conditions of the problem, the model can be implemented.

The 3D model is implemented following the three steps of the 2D model such as: pure diffusion without traps, dislocation simulation and precipitates simulation.

The second model (3D) is implemented in Ansys Workbench, in particular the FEM model APDL is used to parametrize the simulation. In this simulation thermal analysis module was used for the hydrogen diffusion.

The first model is the simplest one and is based on the hydrogen pure diffusion in a truncated octagonal shape, surrounded by the boundary grain. So, the only trap for this model is the boundary grain.

The microstructure is formed by a truncated octagonal grain surrounded by grain boundary phase (Fig. 2a-c). The dimension of geometry is reported in Table 2.

The elements of the mesh have approximately the same size and to do it the body sizing tool was used.

The grain and the grain boundary don't have the same behaviour in the diffusion problem, for that reason two different materials are used whose properties are shown in the Table 3.

An uniform temperature of 100 °C was set to simulate a 100% saturation of hydrogen on one face of the truncated octagon.

Table 2
3D model design parameters.

Design parameter	Value
Grain volume [um^3]	185,44
Boundary grain thickness [um]	1,5
Boundary grain volume [um^3]	102,68
Total volume [um^3]	288,12

2. Results and discussion

Figure 2d shows the nodal solution of the pure diffusion simulation in the first model.

From the nodal solution of the 3D simulation, it's possible to observe that:

1) Hydrogen atoms diffuse through a grain from surface towards grain interior. Precisely, the easiest available sites of the materials namely normal interstitial sites and grain boundaries are firstly occupied;
2) Hydrogen diffuses at different rates depending on the properties of the material used.
3) The maximum concentrations of hydrogen occur in the grain boundary, that is completely saturated and represents the preferential diffusive path;
4) Compared to other kind of sites for occupancy of hydrogen, trapping sites such as grain boundaries seems to provide an energetically favourable environment for occupancy by the hydrogen atoms;
5) In the lattice, the concentration of hydrogen is directly proportional to the distance from the grain boundary. The highest concentrations occur near the edge; and more time of diffusion is required to saturate the lattice core.

Table 3
Material properties for the 3D model.

Material Name	Mat ID	Density, ρ [$\frac{kg}{um^3}$]	Specific Heat, cp [$\frac{pj}{kg\ K}$]	Conductibility coefficient, KXX [$\frac{pW}{um^3 K}$]
Lattice	1	1	1	0,00,014
Boundary grain	2	1	1	0,14
Dislocation	3	1	1	0,014
Precipitates	4	1	1	0,00,014

To complicate the simulation and make it more accurate the implementation of traps such as dislocations and precipitates is needed.

The first type of trap that will be implemented are dislocations. Table 4 summarized the dislocation calculation for a temperature equals to 300 K.

Knowing the number of elements N_{disl}, it's possible to update the model by adding the material of the dislocation and the dislocation elements.

The results of the new simulation are shown in Fig. 2e.

From nodal solution of the dislocation simulation, it's possible to observe that:

1) The presence of dislocation as a reversible trap has a strong effect on the hydrogen trapping;
2) Diffusion path in lattice is highly influenced by the dislocation's elements, in particular dislocation accelerate the diffusion in the lattice thanks to lower binding energies;
3) Boundary grains have still the maximum hydrogen concentration;
4) Individual dislocations which mostly reside in the grain interior can act as a hydrogen trap just as much as those in collective arrangements into low-angle grain boundaries;
5) Hydrogen concentration in lattice is still dependent on the distance from the boundary grain, but the dependence from dislocation effect is greater. Because the saturation of the grain is strongly asymmetry.

The last type of traps that is analysed are the precipitates.

Since precipitates are irreversible traps, it is necessary to know how many of these traps are saturated. To solve this problem, macros have been implemented that analyse the concentration of hydrogen before the generation of precipitates. If the hydrogen concentration is higher than the limit that makes the precipitate saturated, then the mesh around the precipitate is refined to simulate the saturation effect.

It is possible that not all precipitates are saturated, for this reason and to lighten the computation load of the model, the saturated precipitates will be meshed. Precipitates are of four different categories, so four limiting concentrations are used for calculations in macros. The first simulation (no precipitates) contains only the grain boundary and the dislocations as traps.

Knowing number of the saturated precipitates the mesh is updated to considering the precipitate effect.

It seems that the precipitates traps act as secondary sites trapping hydrogen once the reversible trapping sites are filled. It is probably due to higher binding energies.

The main effects of the precipitates occur in the grain boundary (higher saturation level), in particular the elements of the precipitates have lower saturations than those of the grain boundary. Indeed, due to more atomic disorder at/vicinity of grain boundaries, the possibility of the formation and accumulation of nano/macro voids at the grain boundaries increases which in turn provide less coherent interfaces between precipitate/matrix. It is worth noting that hydrogen will tend to concentrate at less coherent interfaces.

A circular pattern of hydrogen diffusion is seen around the precipitates. It is probably related to the matrix distortion observed around precipitates. Furthermore, the presence of such lattice distortion probably creates micro voids due to the high degree of misorientation of the nearby matrix, which in turn contribute to making higher saturation level of hydrogen.

Table 4
Dislocation design parameters for the 3D model.

Design parameter	Value
Dislocation density $[\frac{1}{m^2}]$	10^{16}
Dislocation length [pm]	160,000
Number of hydrogen atoms that fill all the dislocations	$5.76 * 10^9$
Dislocation number of elements, N_{disl}	2019

To make a better implementation of a microstructure, several grains was considered.

The microstructure in the simulation is formed by 17 truncated octagon grains surrounded by grain boundaries phases.

The geometry analysed in the model is composed by 184 grains. The volume is formed by a cube in which 9 grains are placed on each side.

The geometry was chosen to analyse the phenomenon of diffusion on an adequate scale in order to obtain physically acceptable results from the model.

It is necessary to mesh first the grain boundary and then the grain. Using this meshing method, it's possible to get that the ID number of the first elements and nodes belongs to the grain boundary, the second group of elements and nodes belongs to the grain. Figure 3 shows the mesh implementation. Table 5 shows the summarized results for the mesh calculation.

The first Macro that is generated is called ``EXPORT NUMBER OF NODES AND ELEMENTS''. This macro is written in APDL, and it's able to export all the mesh statistics from the Ansys model to texts files. After the export it's possible to manipulate the results to generate the precipitates and the dislocation elements.

The code will automatically calculate the hydrogen diffusion coefficient for all the material by using the working temperature.

A code implemented by Python ("DISLOCATION") reads all the results exported by [Appendix 1] and the input data from the Interface to calculate the number of elements that will simulate the dislocation effects.

This script generates the input for the second Python script. In this file there are the total elements number for the geometry, the element number for the boundary grain, the total node number for the geometry, the node number for the boundary grain and the element number for the dislocation. it is used to decrease the level of mathematical calculation that each script has, because the export procedure of the number of elements and nodes from Ansys Workbench and the reading of these files are the slowest processes of the whole model.

The second script is called ``dislocation generation''. This code can read the output of the "DISLOCATION" script and generate a macro in APDL who can be read by Ansys Workbench to implement the dislocation. In this code the number of elements of the dislocation is read and

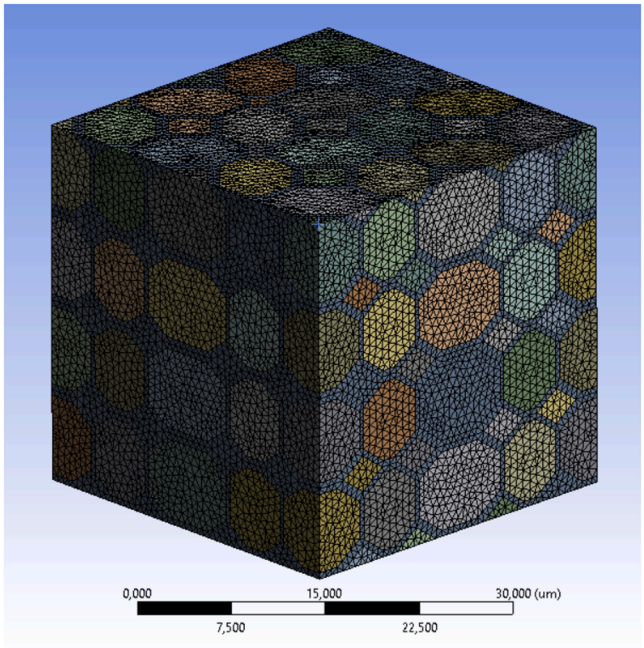

Fig. 3. 3D final mesh.

Table 5
Mesh design parameters.

Mesh parameter	Value
Total number of nodes	1,064,991
Total number of elements	777,753
Grain number of nodes	889,186
Grain number of element	567,995
Boundary grain number of nodes	386,099
Boundary grain number of element	209,758

Table 6
Precipitate calculation results.

Type of precipitate	Number of nodes in boundary grain	Number of nodes in grain	Total number of nodes	Total number of saturated nodes
G1	1210	518	1728	168
G2A	3124	1339	4463	464
G2B	1578	677	2255	334
G3	414	177	591	121

it's converted to number of nodes. Knowing the number of the nodes of the dislocation it's possible to generate the macro who creates the dislocations in the grain. The ID number of the nodes in the grain are chose randomly. The output generated by this script is a macro called ``ND_disl'', whit this macro it's possible to create named sections who will represent the node of dislocation and the element of dislocation, this macro changes the material properties of the dislocation elements. [Appendix 2].

After the mesh updating it's necessary to launch the first transient thermal simulation. The behaviour of the microstructure is simulated as a consequence of a hydrogen saturated atmosphere adjacent to one side of the geometry, where concentration is equal to 100%.

The nodal results must be exported as a text file for the consistency of the model, it's necessary to create a text file called "SATURATION_NODE_0.txt" [Appendix 3].

The presence of an extra half-plane of atoms called dislocation in an ordered planes of a materials provide internal strain that effectively beneficial in hydrogen trap density. One can be found that solute hydrogen effectively increases the velocity of dislocations and facilitate the propensity for edge character dislocations. The presence of such crystalline defects not only probably change the fracture mode but also strongly enhances hydrogen trap density by the hydrostatic stress field of edge dislocations. Moreover, the simulated results and video clips provided in Supplementary materials 2, is observed that hydrogen-concentration heterogeneities can eliminate with time by the concentration gradient diffusion. Specifically, owing to the ability of dislocation to move and carry hydrogen, higher dislocation density means bigger dislocation mean free paths, and consequently higher hydrogen concentrations. In addition, considering fast hydrogen diffusion at high-angle grain boundaries as normal grain boundaries compared to low-angle grain boundaries typically forming by rearranged dislocations inside the grains, the permeation rate of hydrogen increases from the grain boundaries to the grain interior. The dislocations rearrange in the form of LAGBs, resulting in an apparent decrease of the residual stresses which in turn absorb less hydrogen. It seems that higher density of reversible traps such as dislocations reduces the hydrogen permeability and diffusivity and also increases apparent solubility of hydrogen in steels.

The effect that precipitates have in the simulation was implemented by macros in Python, that import the results of the previous section (operating temperature, number and ID of the elements of dislocation and nodal results).

The 70% of the total precipitates are in the grain boundary, other 30% is in the grain. Knowing the maximum concentration of hydrogen that each precipitate can contain; it is possible to know the number of saturated precipitates.

A macro was generated in order to create components in Ansys Workbench that contain the nodes and elements of each type of precipitate. This macro is called "PRECIPITATES". [Appendix 4] For this macro it's used a Fortran format descriptors "8i10". Table 6 summarized the results for the precipitates calculation. For different type of precipitates, different saturated nodes are achieved so that 10%, 10%, 12% and 20% of saturated nodes calculated for G1,G2A,G2B and G3, respectively. As average diameter of the precipitates decreases, in turn, the number of saturated precipitates increase which in turn causes the increase the maximum concentration of hydrogen. It seems that less trapping energy of smaller precipitates such as G3, compared to larger ones such as G1, strongly affect the amount of the trapped hydrogen. Since the spherical assumption was adopted for the geometry of all the precipitates, it can be inferred that the type of interface formed between precipitates with the matrix is effectively impact on the number of saturated sites of hydrogen.

The thermal simulation was started with the same settings of the last simulation. The nodal results must be exported as a text file for successive analysis, it's necessary to create a text file called "SATURATION_NODE_1.txt" [Appendix 5].

Figure 4 shows the nodal solutions for the total geometry during the simulation.

The simulated geometry has a volume of 28,668 [um^3]. All saturation curves simulate the average evolution of hydrogen saturation for the volume of the geometry. A saturation equal to 100% indicates that the entire volume has reached the maximum capacity of hydrogen atoms. Figure 5a shows the trend of the average saturations for grain boundary, grain and dislocations for a time interval ranging from 0 s to 25000s. The average saturation of the grain boundary at the end of the simulation reaches a value of 84.9%. This value is based on the grain boundary volume which is 6967 [um^3]. The mean saturation curve of the grain boundary tends fastest to the horizontal asymptote representing the full saturation value (100%). The second fastest saturation curve is that of the dislocations. At the end of the simulation (25000s) the dislocations reach an average saturation level of 83.5% (based on a volume of 2170 [um^3]). The saturation curve of the lattice is the least rapid, at the end of the simulation (25000s) a maximum saturation level of 81.1% is reached on a volume of 21,701 [um^3]. The global saturation curve is strongly dependent on that of the grain due to its volume, in fact the volume of the grain is equal to 75% of the total volume. At the end of the simulation the global saturation is 81.8%.

The results demonstrate austenitic microstructure possess grain boundaries, dislocation, and the precipitates have a descending priority to fill out by hydrogen atoms. Moreover, a higher volume of hydrogen permeation at longer times in the microstructure is achieved based on the Fick's law. This time dependence of hydrogen diffusivity strongly depends on the type of trapes, where grain boundaries, dislocation and then lattice could provide the highest saturation of hydrogen. It is shown in Fig. 8 (b) that the time needed to reach the saturation steady state at grain boundaries is shorter compared to dislocations and lattice respectively. This can be easily understood as it will take less time to reach the steady state hydrogen saturation when the average bulk hydrogen concentration surrounding the grain boundaries is further compared to dislocation and lattice. Specifically, larger conductivity coefficient of grain boundaries easily means higher and faster mass diffusion of hydrogen at the grain boundaries.

Subsequently, the minimum saturation change in the microstructure is analysed. With this analysis it is possible to obtain the saturation trend of the microstructure portions which are last reached by the hydrogen diffusion path. The changing in the minimum saturation in the microstructure is analysed, so it is possible to obtain the saturation trend of the microstructure portions which are last reached by the hydrogen diffusion path. The grain boundary is the portion of the volume that first diffuses the hydrogen, by analysing the minimum saturation curves it is

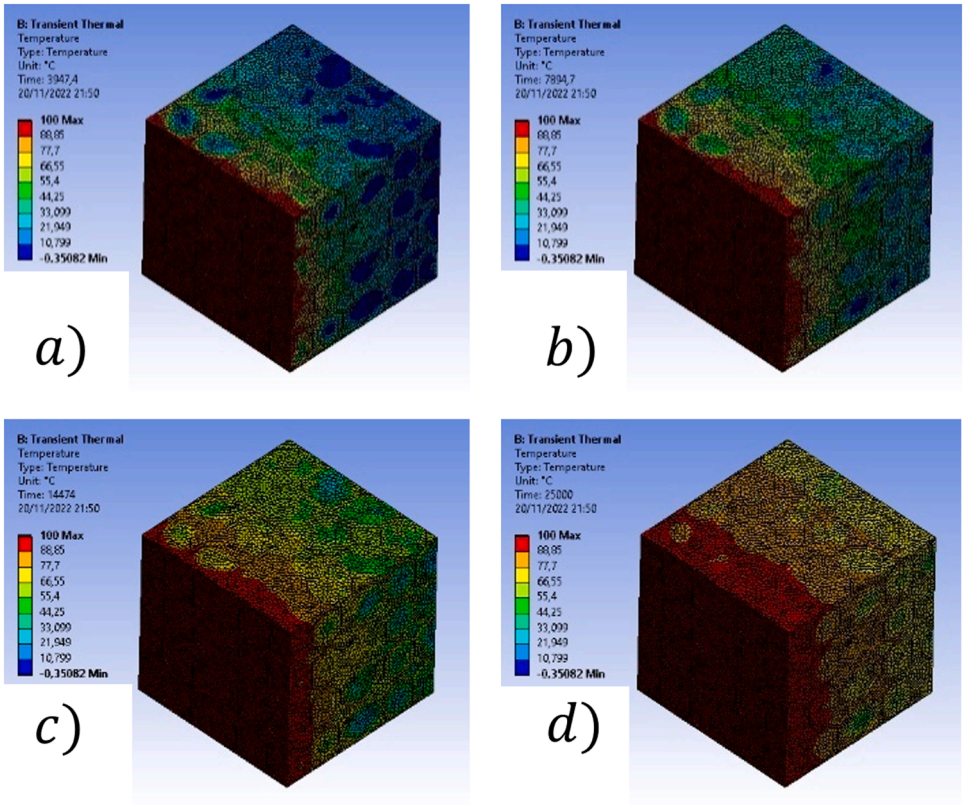

Fig. 4. Hydrogen saturation evolution; a) 4000 s; b) 8000 s; c) 14000s; c) 25000s.

possible to notice that the minimum saturation value in the grain boundary increases rapidly with time, in fact after 5000 s the minimum saturation value of all the volume of the grain boundary is 20%. After 5000 s of simulation the minimum saturation value in the grain and in the dislocations does not exceed 5%. To obtain a minimum saturation value of 20%, it takes 14000s for the dislocations and 17000s for the grain, respectively. The minimum saturation trend of the entire microstructure is superimposed on that of the lattice, this effect occurs because the lattice is the largest volumetric portion within the microstructure. . It is inferred that the hydrogen saturation limit is directly related to the presence of lattice defects. Therefore, it is found that the volumetric portion within the microstructure plays a significant role on the saturation status and permeation behaviour.

The final performed simulations concern the analysis of the effectiveness of the model for simulations carried out at various working temperatures. Since the diffusive coefficient of the grain boundary increases with the increase of the absolute temperature, the saturation trend is consistent with this physical concept. In particular, the average saturation of the grain boundary has a percentage increase of 8.7% for a temperature of 75 °C and an average percentage increase of 11.4% for a temperature of 150 °C (respect to 25 °C). These temperatures have been chosen based on the thermal range to which an austenitic stainless steel is subjected. At a given time, the grain boundaries provide more saturation thank to high-speed and high flux permeation of hydrogen due to the coexistence of a high diffusion coefficient of grain boundaries and supply of hydrogen from the surrounding grains. Considering the Fick's law, diffusion coefficient strongly depends on temperature and time, and consequently at higher temperature, the time needed to saturate is less.

The average saturation of the grain has a percentage increase of 4.1% for a temperature of 75 °C and an average percentage increase of 6.4% for a temperature of 150 °C.

The results show that grain saturation is less affected by the increase in temperature than boundary grain.

The number of dislocations depends on the temperature, as the temperature increases there is a decrease in the number of dislocations. However, the decrease of the elements of the dislocations is accompanied by an increase in the diffusion coefficient of the dislocations themselves. Thus, even though the number of dislocations is decreasing, their saturation level increases with temperature. From one side, higher local grain boundaries energy and higher free volume at the grain boundaries for hydrogen trapping, and from other side, suitability of dislocation cores in the grain volume as another potential trapping site results in achieving higher and faster hydrogen saturation in the lattice. Furthermore, the results show that grain saturation is less affected by the increase in temperature than boundary grain.

The number of precipitates is considered fixed as the temperature varies, however as the temperature increases there is an increase in the diffusion properties of the entire microstructure, this increase favours the saturation of the precipitates which as the temperature increases tend to be all saturated with hydrogen [47]. The longer time and lower amount of hydrogen saturation for the case where the precipitates are present is due to the higher hydrogen trapping energy around the precipitates compared to the other structural defects.

Figure 5b shows the trend of the global saturation variation. It is obvious, that the amount of possibly trapped hydrogen Arrheniusly increased with increasing temperature. This effect is not surprising at all, because the mobility of hydrogen atoms increases as a consequence of higher temperature and energy barriers can be overcome more easily. Comparing the plots demonstrate at low temperatures, there is a greater sensitivity to hydrogen saturation compared to higher temperatures regardless of the type of structural defects. Moreover, it is noteworthy that the presence of precipitates has a more significant effect on the amount of hydrogen saturation compared to the corresponding saturation time. Increasing temperature results in loss of the coherency of interfaces formed between precipitates and matrix which in turn strongly affect as negatively on hydrogen adsorption at grain boundaries and dislocations.

Table 7 shows the times necessary for the maximum saturation of the

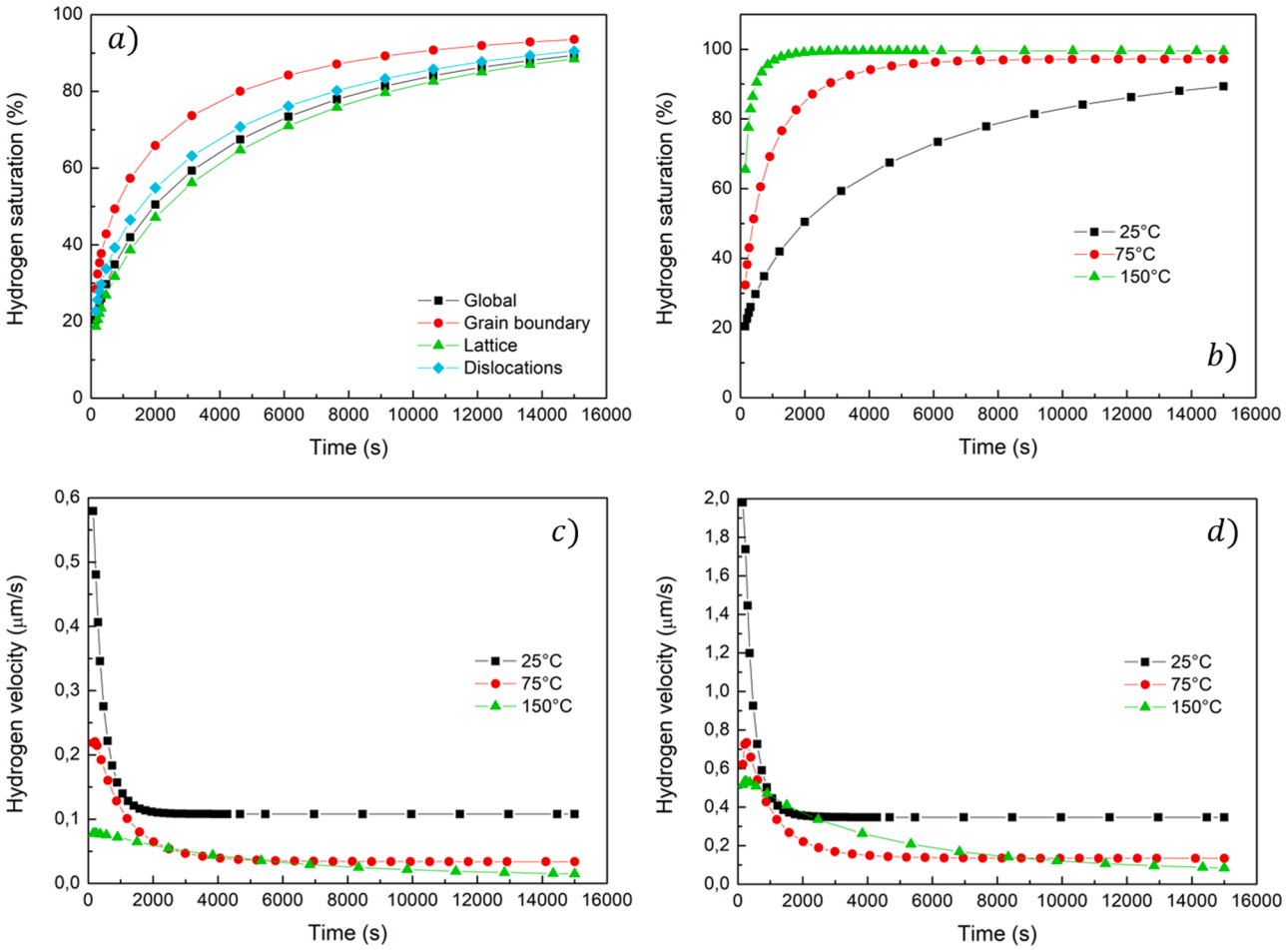

Fig. 5. Saturation curves of the final model (a), level of global saturation in function of the temperature (b), hydrogen velocity in grain boundary-grain interface (c), hydrogen velocity in dislocation-grain interface (d).

Table 7
Saturation time in function of the temperature.

Temperature [°C]	Saturation time [s]
25	20,000
75	8000
150	2000

simulated geometry as a function of time. Using these values, it is possible to trace a trend of the total saturation times of the simulated geometry as a function of time and temperature.

Figure 10 shows the average velocity of hydrogen particles passing through the grain boundary interface in function of the time. The calculation is made with the following assumptions:

$$c_{p_H} = 14,304 \left[\frac{j}{kgK}\right]$$

$$\rho_H = 0.0899 \left[\frac{kg}{m^3}\right]$$

$$v_{m_H} = 11.42 * 10^{-3} \left[\frac{m^3}{mol}\right]$$

$$A_{Lat_{GB}} = 2425.5 \left[um^2\right]$$

where c_{p_H} is the hydrogen specific heat, ρ_H is the hydrogen density, v_{m_H} is the hydrogen molar volume and $A_{lat_{GB}}$ is the area of the interface between grain and boundary grain. Fig. 5c shows the results for three temperatures (25 °C, 75 °C and 150 °C). The velocity profile of the flow of hydrogen atoms in surface A passing from the grain boundary to the grain decreases with increasing time. This phenomenon is due to the increase in saturation of the microstructure with the time which requires less flow of hydrogen with increasing time (to saturate the model). The mean speed of the flow increases with the increase of the temperature and with it also the modulus of the asymptotic value to which it tends. The tendency to absorption of hydrogen in easy-accessible and thermodynamically perfectional sites, namely grain boundaries and interfaces, can undergo occupation over time. The most important reason for such saturation is the low packing essence of the such regions, which can be significant considered for trapping hydrogen atoms. Although it seems that the passage of time can reduce the concentration gradient of hydrogen in the interface areas towards the inside of the grain. It is noteworthy that these changes are intensified at higher temperatures due to their inherent dependence on atomic penetration, so that hydrogen atoms penetrate into the grain at higher temperatures at a faster rate than the interface areas.

Figure 5d shows the average velocity of hydrogen particles passing through the dislocation-grain interface. As temperature increases to 75 °C, the lattice dislocation can dissociate or redistribute itself into low angle GB which more likely possess stronger trapping effect compared to individual dislocations. By proceeding the increase temperature to 150 °C not only effectively release dislocations from more tangling, but also increase the hydrogen diffusivity throw-outs microstructure. In this case the value of the mean velocity is greater than the value of the boundary grain-grain interface. In this case the value of the mean

velocity is greater than the value of the boundary grain-grain interface.

The hydrogen flow rate has the same trend of the hydrogen velocities. Also, in this case the explanation for this phenomenon is the global increase in saturation over time. this increase leads to a reduction in the speed and flow rate of hydrogen in the microstructure. The flow rate of hydrogen tends to decrease until it stops for the time of complete saturation. By and large, it can be concluded that as temperature increases, hydrogen embrittlement susceptibility is promoted. It is due to a decrease in the hydrogen effusion to the surface of the material and the preserve of a significant amount of hydrogen in the structural defects such as grain boundaries, dislocation and precipitates by temperature effect.

An error analysis was performed to verify that the generated model is mathematically correct. To do this, it is necessary to compare the values of the nodal temperatures around the precipitates before and after the implementation of the latter. An error of less than 7% is considered acceptable for this type of analysis.

The error analysis was carried out for three temperatures in order to have a trend of the robustness of the model as a function of the temperature. From the error analysis it emerges that the model has an error of less than 3% in all the simulated temperatures. This result demonstrates the reliability of the model as the temperature varies.

The simulations movies describing the diffusion behaviour are shown in Supplementary material 2.

3. Conclusions

The model simulates the diffusion of hydrogen in an austenitic stainless-steel microstructure. It is possible to modify the material properties to simulate the diffusion of hydrogen for various types of microstructures. Three different grain sizes have been implemented in the model, by modifying the geometry it is possible to simulate the diffusion of hydrogen for grains of different sizes and shapes in such a way as to adapt the model to the desired microstructure. It is possible to implement microstructures with asymmetric grains and of various crystalline structures. This analysis can set the basis to better hydrogen storage, that represents a big limit in the use of this kind of energy vector.

Declaration of Competing Interest

The authors declare that they have no known competing financial interests or personal relationships that could have appeared to influence the work reported in this paper.

Acknowledgments

The authors would like to thank the Italian Ministry for University and Research for the fundings provided to “Finanziato dall’Unione europea – Next Generation EU”. Progetto di ricerca dal titolo Sustainable Mobility center (Centro Nazionale per la Mobilità Sostenibile – CNMS) Codice CN00000023, CUP: F83C22000720001.

Supplementary materials

Supplementary material associated with this article can be found, in the online version, at doi:10.1016/j.mtla.2023.101855.

References

[1] H.K. Birnbaum, P. Sofronis, Hydrogen-enhanced localized plasticity-a mechanism for hydrogen-related fracture, Mater. Sci. Eng. A 176 (1–2) (1994) 191–202.
[2] I.M. Robertson, P. Sofronis, A. Nagao, M.L. Martin, S. Wang, D.W. Gross, K. E. Nygren, Hydrogen embrittlement understood, Metall. Mater. Trans. B 46 (2015) 1085–1103.
[3] S. Bechtle, M. Kumar, B.P. Somerday, M.E. Launey, R.O. Ritchie, Grain-boundary engineering markedly reduces susceptibility to intergranular hydrogen embrittlement in metallic materials, Acta Mater. 57 (14) (2009) 4148–4157.
[4] M. Koyama, C. CemTasan, E. Akiyama, K. Tsuzaki, D. Raabe, Hydrogen-assisted decohesion and localized plasticity in dual-phase steel, Acta Mater. 70 (15) (2014) 174–187.
[5] M. Nagumo, M. Nakamura, K. Takai, Hydrogen thermal desorption relevant to delayed-fracture susceptibility of high-strength steels, Metall. Mater. Trans. A 32 (2001) 339–347.
[6] I. Moro, L. Briottet, P. Lemoine, E. Andrieu, C. Blanc, G. Odemer, Hydrogen embrittlement susceptibility of a high strength steel X80, Mater. Sci. Eng. A 527 (27–28) (2010) 7252–7260.
[7] What is hydrogen embrittlement? – Causes, effects and prevention, TWI - The Welding Institute. Accessed 2023.
[8] M.S. Daw, M.I. Baskes, Semiempirical, quantum mechanical calculation of hydrogen embrittlement in metals, Phys. Rev. Lett. 50 (1983) 1285.
[9] R.A. Oriani, Hydrogen embrittlement of steels, Ann. Rev. Mater. Sci. 8 (1978) 327–357.
[10] N.-E. Laadel, M. El Mansori, N. Kang, S. Marlin, Y. Boussant-Roux, Permeation barriers for hydrogen embrittlement prevention in metals – a review on mechanisms, materials suitability and efficiency, Int. J. Hydrogen Energy 47 (76) (2022) 32707–32731.
[11] Yi Liu, Yang Chen, Chendong Yang, Junhe Lian, Yi Feng, Xianhong Han, The effect of charging conditions on hydrogen embrittlement behavior of ultra-high-strength steel 22MnB5, Mater. Charact. 194 (2022), 112377.
[12] Jin Sung Park, Sung Jin Kim, Effects of two-step austenitizing processes on hydrogen evolution, permeation, and cracking behaviors of ultra-high-strength martensitic steel, Mater. Sci. Eng. A 859 (2022), 144214.
[13] L.S. Morrisey, S. Nakhla, Molecular dynamics simulations of the hydrogen embrittlement base case: atomic hydrogen in a defect free single crystal, Molec. Sim. 48 (13) (2022) 1214–1222.
[14] H. Bhadhesia, Prevention of hydrogen embrittlement in steels, ISIJ Int. 56 (2016) 24–36.
[15] O.I. Zvirko, E.I. Kryzhanivskyi, H.M. Nykyforchyn, H.V. Krechkovska, Methods for the evaluation of corrosion-hydrogen degradation of steels of oil-and-gas pipelines, Mater. Sci. 56 (2021) 585–592.
[16] H. Nykyforchyn, O. Tsyrulnyk, O. Zvirko, H. Krechkovska, Non-destructive evaluation of brittle fracture resistance of operated gas pipeline steel using electrochemical fracture surface analysis, Eng. Fail. Anal. 104 (2019) 617–625.
[17] Zhilin Zheng, Min Yi, Shuai Wang, Abnormal trapping of hydrogen in the elastic stress field of dislocations in body-centered cubic iron, Int. J. Hydrogen Energy 47 (92) (2022) 39255–39264.
[18] S. Leitner, W. Ecker, F.D. Fischer, J. Svoboda, Thermodynamic trapping and diffusion model for multiple species in systems with multiple sorts of traps, Acta Mater. 233 (2022), 117940.
[19] C.J. Williams, E.I. Galindo-Nava, Accelerating off-lattice kinetic Monte Carlo simulations to predict hydrogen vacancy-cluster interactions in α-Fe, Acta Mater. 242 (2023) 118452.
[20] R. Fernández-Sousa, C. Betegón, E. Martínez-Pañeda, Cohesive zone modelling of hydrogen assisted fatigue crack growth: the role of trapping, Int. J. Fatigue 162 (2022), 106935.
[21] A. McNabb, P.K. Foster, A new analysis of the diffusion of hydrogen in iron and ferritic steels, Trans. Metal. Soc. 227 (1963) 618–627.
[22] H. Alfons, M. Krom, A. Bakker, Hydrogen trapping models in steel, Metall. Mater. Trans. B 31 (6) (2000) 1475–1482.
[23] Lizeth Sanchez, Hongbo Cong, AC interference on hydrogen absorption in low carbon steel under cathodic protection, Int. J. Hydrogen Energy 48 (3) (2023) 1202–1217.
[24] A. Díaz, A. Zafra, E. Martínez-Pañeda, J.M. Alegre, J. Belzunce, I.I. Cuesta, Simulation of hydrogen permeation through pure iron for trapping and surface phenomena characterisation, Theoret. Appl. Fract. Mech. 110 (2020), 102818.
[25] V.I. mironov, I.G. Emel’yanov, O.A. Lukashuk, Criteria of material failure in relation to hydrogen saturation, Sol. State Phen. 316 (2021) 484–489.
[26] S. Samanta, P. Kumari, K. Mondal, M. Dutta, S.B. Singh, An alternative and comprehensive approach to estimate trapped hydrogen in steels using electrochemical permeation tests, Int. J. Hydrogen Energy 45 (51) (2020) 26666–26687.
[27] O. Barrera, E. Tarleton, H.W. Tang, A.C.F. Cocks, Modelling the coupling between hydrogen diffusion and the mechanical behaviour of metals, Comput. Mater. Sci. 122 (2016) 219–228.
[28] A. Oudriss, J. Creus, J. Bouhattate, E. Conforto, C. Berziou, C. Savall, X. Feaugas, Grain size and grain-boundary effects on diffusion and trapping of hydrogen in pure nickel, Acta Mater. 60 (19) (2012) 6814–6828.
[29] C. Marte, R. Kirchheim, Hydrogen diffusion in nanocrystalline nickel indicating a structural change within the grain boundaries after annealing, Scr. Mater. 37 (8) (1997) 1171–1175.
[30] Y.-L. Liu, Y. Zhang, H.-B. Zhou, G.-H. Lu, F. Liu, G.N. Luo, Vacancy trapping mechanism for hydrogen bubble formation in metal, Phys. Rev. B 79 (17) (2009), 172103.
[31] T. Hickel, R. Nazarov, E. McEniry, G. Leyson, B. Grabowski, J. Neugebauer, Ab initio based understanding of the segregation and diffusion mechanisms of hydrogen in steels, JOM 66 (8) (2014) 1399–1405.
[32] J. Hirth, B. Carnahan, Hydrogen adsorption at dislocations and cracks in Fe, Acta Metall. 26 (12) (1978) 1795–1803.

[33] A. Oudriss, J. Creus, J. Bouhattate, C. Savall, B. Peraudeau, X. Feaugas, The diffusion and trapping of hydrogen along the grain boundaries in polycrystalline nickel, Scr. Mater. 66 (1) (2012) 37–40.
[34] M. Nagumo, Fundamentals of Hydrogen Embrittlement, Springer, Singapore, 2016.
[35] A. Azócar Guzmán, J. Jeon, A. Hartmaier, R. Janisch, Hydrogen embrittlement at cleavage planes and grain boundaries in Bcc iron—revisiting the first-principles cohesive zone model, Materials (Basel) 13 (24) (2020) 5785.
[36] S. Ueki, R. Oura, Y. Mine, K. Takashima, Micro-mechanical characterisation of hydrogen embrittlement in nano-twinned metastable austenitic stainless steel, Int. J. Hydrogen Energy 45 (51) (2020) 27950–27957.
[37] L. Coudreuse, A.-M. Brass and J. Chêne, Techniques de l'ingénieur Corrosion et vieillissement: phénomènes et mécanismes base documentaire : TIB371DUO (ref. article : m176) (2000).
[38] H. Swan, P. Styman, H. Wilcox, N. Bowden, T. Ungar, L. Connor, A. Garner, A. Cole-Baker, P. Binks, C. Smith, S. Sikotra, J. Hawes, S. Ortner, Measurement of hydrogen trapping in cold-work dislocations using synchrotron X-ray diffraction, J. Nucl. Mater. 571 (2022), 154012.
[39] E.C.E. Rönnebro, R.L. Oelrich, R.O. Gates, Recent advances and prospects in design of hydrogen permeation barrier materials for energy applications—a review, Molecules 27 (19) (2022) 6528.
[40] R.A. Oriani, P.H. Josephic, Equilibrium aspects of hydrogen-induced cracking of steels, Acta Metall. 22 (9) (1974) 1065–1074.
[41] B. Zhang, M. Asta, L.-W. Wang, Machine learning force field for Fe-H system and investigation on role of hydrogen on the crack propagation in α-Fe, Comput. Mater. Sci. 214 (2022), 111709.
[42] L. Borja Peral, I. Fernández-Pariente, C. Colombo, Critical hydrogen concentration for crack propagation in a CrMo steel: targeted experiments for accurate numerical modelling, Eng. Fract. Mech. 273 (2022), 108764.
[43] M. Connolly, V. Malavé, M.L. Martin, Hydrogen concentration-induced stresses in an environmental TEM, Phys. Rev. Mater. 6 (2022), L040601.
[44] M. Asadipoor, A. Barnoush, Assessment of hydrogen embrittlement on advanced high strength steels revealed by in-situ electrochemical micro-cantilever bending test, Int. J. Hydrogen Energy 47 (17) (2022) 10112–10121.
[45] N.Z. Carr, R.B. McLellan, Hydrogen-vacancy interactions in Ni-H solid solutions, J. Phys. Chem. Solids 67 (8) (2006) 1797–1802.
[46] K. Takai, H. Shoda, H. Suzuki, M. Nagumo, Lattice defects dominating hydrogen-related failure of metals, Acta Mater. 56 (18) (2008) 5158–5167.
[47] B.O. Hoch, Modelling of hydrogen diffusion in heterogeneous materials: implications of the grain boundary connectivity, Materials. Université de La Rochelle (2015). English. ffNNT:2015LAROS030ff.